

Article

Hydrodynamic Controls of Particulate Metals Partitioning along the Lower Selenga River—Main Tributary of The Lake Baikal

Sergey Chalov ^{1,*} , Vsevolod Moreido ², Ekaterina Sharapova ¹, Lyudmila Efimova ¹, Vasyli Efimov ¹, Mikhail Lychagin ¹ and Nikolay Kasimov ¹

¹ Faculty of Geography, Lomonosov Moscow State University, 119991 Moscow, Russia; koshakosha97@gmail.com (E.S.); ef_river@mail.ru (L.E.); roxifixat@yandex.ru (V.E.); lychagin2008@gmail.com (M.L.); nskasimov@mail.ru (N.K.)

² Water Problems Institute of Russian Academy of Sciences, 119333 Moscow, Russia; vsevolod.moreydo@iwp.ru

* Correspondence: srchalov@geogr.msu.ru; Tel.: +74-9-5939-1552

Received: 25 March 2020; Accepted: 5 May 2020; Published: 9 May 2020



Abstract: In this study, the downstream effects of pollutants spreading due to hydromorphological gradients and associated changes in sediment transport conditions along the braided-meandering and deltaic distributary reach of a large river downstream section are discussed. We demonstrate the significance of hydrodynamic control for sediment-associated metal partitioning along the river. Typically, the downward decline of the sediment and metals spreading towards Lake Baikal is observed due to buffer effects in the delta. During peak flow, the longitudinal gradients in heavy metal concentration along the distributary delta reach are neglected due to higher concentrations delivered from the upper parts of the river. In particular, significant variations of heavy metal concentrations associated with the river depth are related to sediment concentration and flow velocity profiles. Various particulate metal behavior in silt-sand delta channels and the sand–gravel Selenga main stem emphasize the importance of near-bottom exchange for particles spreading with the river flow. Using empirically derived Rouse numbers, we found quantitative relationships between the ratio of particulate metals sorting throughout depth in a single river channel and the hydrodynamic conditions of sediment transport.

Keywords: sediment sorting; Rouse number; particulate metals; Selenga; Lake Baikal

1. Introduction

River sediments carry tremendous quantities of chemicals and thus act as the main driver of pollution to the recipient lakes and seas [1,2]. Most of the existing studies of suspended sediment geochemistry rely on sediment samples taken at the surface of the river channel, at one single sampling time [3,4]. However, particulate element sorting may exist due to hydrodynamic effects (e.g., velocity, transport capacity) or due to composition (chemistry, mineralogy, size) of grains—both impacts are unknown. Chemical effects of hydrodynamic sorting within the river water column may significantly influence estimates of riverine fluxes and thus require applications of hydrodynamic methods [5,6].

Hydrodynamic sorting of sediments abruptly changes along the lower reaches of large rivers where a decrease of sediment and metal spreading is observed due to channel gradient decline towards the receiving water body related to buffer effects in the delta. For this study, we took the case of the main tributary of the Lake Baikal—the Selenga River, its delta, and adjacent upstream 100 km reach. Here, the shift from single-channel reach located upstream from the delta to the huge distributary system occurs, which provides an opportunity as a unique field laboratory to explore varying hydrodynamic

effects on sediment transport and composition. Physical controls on spatial transitions in bed material from gravel to sand have been discussed before [7,8], demonstrating relations of distribution of sediment grain size in deltaic channels and hydrodynamics and sediment transport conditions. At the same time, the transition of sediment fluxes, including partitioning between suspended load and bedload, as well as the hydrodynamic drivers of geochemical fluxes, remains unclear.

In this paper, we investigate hydromorphological gradients and associated changes in sediment transport conditions in the braided-meandering and distributary reach of the large Selenga river downstream section. We argue that the well-known Rouse model [2] of sediment transport [2], both with the suspended particulate matter concentration profiles, predicts suspended load to bedload partitioning and can be used as a proxy to describe particulate metal transport as a function of height above the bed from a limited number of measured parameters: suspended sediment concentration at a given depth, particle size distribution, and bottom shear velocity. The particular focuses of the paper are (1) downstream variations of sediment transport conditions and partitioning between suspended load and bedload, (2) the effects of these processes into particulate concentrations of metals during a particular flood event of 2018, and (3) the behavior of chemical elements with respect to hydrodynamic sorting within the river water column along the river course.

2. Data and Methods

The case study is the Selenga River, originating in Mongolia, which contributes about 50% of the total inflow into Lake Baikal and is considered as a key sustainability factor of the largest freshwater lake in the world [9]. Due to the lithochemical features of the lower Selenga basin, its waters are enriched with chemical elements (Fe, Zn, Mo, Cu), with concentrations corresponding to world-average values [10]. The main sources of river pollution are associated with the poorly treated industrial and municipal wastewaters from Ulan-Ude, Selenginsk, and Kabansk cities [11], as well as from cities of Mongolia [12]. The large inland delta (over 500 km²) is considered as an important geochemical buffer to protect Lake Baikal [13,14]. It is a fluvially dominated fresh-water system that is characterized by up to eight orders of distributary channels [7,15–17]; as such, the delta region has developed large lakes and widespread wetland regions that are adjacent to the channels [8,13,18–20]. Here, a significant part of the suspended and dissolved forms of heavy metals and metalloids, coming from various sources, are stored in the delta [13,14,18,21,22]. Previously, a decrease in concentrations of Cu, Pb, Zn in delta reaches, and Mn and Fe in bottom sediments was observed [13,23].

2.1. Sampling and Samples Processing

A hydrochemical screening campaign was carried out between 27 July and 1 August 2018. The measurement transects were distributed 150 km along the lowermost reach of the Selenga River (Figure 1).

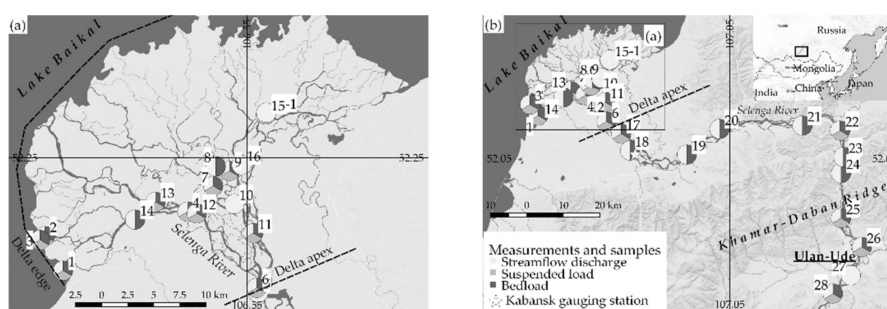


Figure 1. Location of the sampling transects ((a)—delta, (b)—whole reach) during the 2018 field campaign (transect number is given next to its location). Colors in the circle sectors represent the type of samples taken at the specified transect.

This reach is specific for varying conditions with respect to flow hydraulics. The main course of the Selenga River in its lower reach (100–150 km from the Lake Baikal) crosses the Khamar-Daban ridge, flowing in a narrow V-shaped valley in a north direction, and rarely braiding. The top of this reach is where the main source of water pollution from domestic effluent and industrial wastewater—Ulan-Ude city—is located. Next, the river course rotates to the west and enters a vast flatland. Active braiding starts about 40 km from Lake Baikal, where the river forms a delta. The reach upstream from the delta will hereafter be referred to as “main channel” (transects from S18–17 to S18–28 in Figure 1) in contrast to “delta channels” (transects from S18–4 to S18–16 in Figure 1) and “delta edge” (transects S18–1, S18–2, and S18–3 in Figure 1). The latter transects correspond to the lowermost locations within delta channels in the interface between river and lake.

To assess the chemical concentrations and fluxes associated with the bed and suspended sediments, water sampling was carried out on 28 transects along with the simultaneous discharge measurements with an acoustic doppler current profiler (ADCP) to account for local hydraulic conditions. We used a Teledyne RD Instruments RioGrande WorkHorse 600 kHz ADCP (Teledyne RD Instruments USA, 14020 Stowe Drive, Poway, CA 92064, USA) unit mounted on a moving boat. Water samples were pumped out with a filterless submersible 12V pump from three layers (top, midsection, and near-bottom) to account for the vertical distribution of the suspended sediment. For each sample in a depth profile, the boat was repositioned at its original location, and sampling was performed while drifting at the river water velocity.

Bottom sediment samples were taken using a tethered flow-through sampler: an O-shaped metal pipe with a textile filter attached at the rear end. Three samples were taken at each transect—two under each bank and one at the deepest section.

The sampling was carried out during the peak of a flood event (Figure 2). The maximum streamflow discharge calculated from the stage-discharge curve at the Kabansk gauging station (5 km upstream of the delta apex, see Figure 1) on 29 July reached 2390 m³/s. The water stage at this gauge rose nearly 1.5 meters from the beginning of the flood event (Figure 2), leading to bankfull conditions at the delta channels. Due to this fact, transects within Selenga delta were measured under 2000–2200 m³/s water discharges of the Selenga main stem, whereas the upper reach was surveyed under 1800–2000 m³/s.

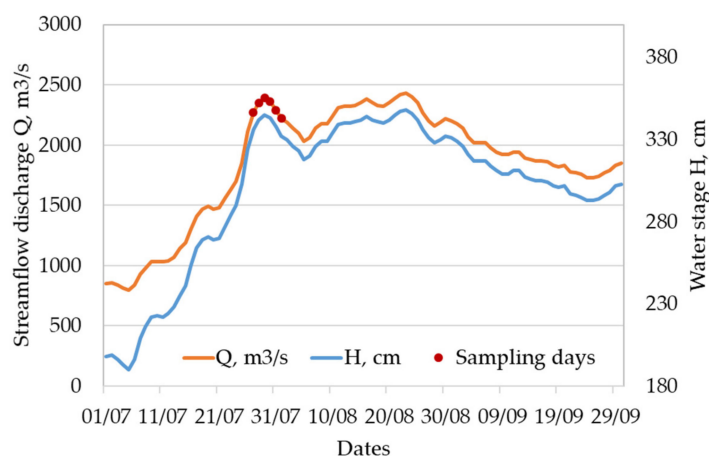


Figure 2. Streamflow hydrograph at Kabansk gauging station during July–September 2018.

2.2. Hydrodynamic Modelling of Sediment Transport

The hydrodynamic conditions of sediment transport and particulate geochemistry evolution along the Lower Selenga River were estimated using based on one-dimensional momentum balance approach, which enables us to calculate bed shear stress condition [24]:

$$\frac{\partial U}{\partial t} + U \frac{\partial U}{\partial x} = -g \frac{\partial \eta}{\partial x} - g \frac{\partial H_{bf}}{\partial x} - \frac{\tau_{bf}}{\rho g} \quad (1)$$

where U is measured depth-averaged flow velocity in the flow direction (x), τ_{bf} is bankfull shear stress, ρ is the density of water, g is gravitational acceleration, and $\frac{\partial \eta}{\partial x}$ is the change in bed elevation in the x -direction. Assuming incompressible, quasi-steady, one-dimensional flow ($\frac{\partial(UH)}{\partial x} = 0$, $\frac{\partial U}{\partial t} = 0$), Equation (1) is reduced to

$$S_f = -\frac{\partial \eta}{\partial x} - \frac{\partial H_{bf}}{\partial x} (1 - Fr^2) \quad (2)$$

$$\tau = \rho g H S_f \quad (3)$$

where S_f is the friction slope and Fr is the Froude number, equal to U / \sqrt{gH} . Shear velocity (V_*) is then equal to

$$V_* = \sqrt{gHS} \quad (4)$$

The precise estimates of bed shear velocity u^* and shear stress τ_b were done based on ADCP [25]:

$$u^* = \frac{\bar{u} \cdot k}{\ln\left(\frac{H}{e \cdot z_0}\right)} \quad (5)$$

where \bar{u} is the integrated velocity of the flow at the sampling site taken from the ADCP measurements, k is von Karman's constant assumed equal to 0.40, H the water depth at the sampling site, e is the base of natural logarithms, z_0 is bed roughness calculated as $z_0 = 0.1 \cdot d_{84}$. Local boundary shear stress values τ_b at the sampling verticals was based on the method by [26]:

$$\tau_b = \rho \left[\frac{ku}{\ln\left(\frac{z}{z_0}\right)} \right] \quad (6)$$

where ρ is the water density assumed unity, k is von Karman's constant assumed equal to 0.40, u is the near-bed velocity, z is the depth at the sampling point, and z_0 is the bottom roughness scale calculated as $z_0 = 0.1 \cdot d_{84}$. A dimensionless Rouse number (Ro) is used to determine conditions of sediment transport and was used as a proxy to explain sediment geochemistry:

$$Ro = \frac{\omega_s}{\beta k V_*} \quad (7)$$

where k is von Karman's constant (0.41), ω_s is settling velocity (m/s) of the bottom sediments, which is a function of grain size, shape, and density) [27]. Settling velocity (ω_s) of natural sediment particles is based on methods presented by Dietrich and is estimated with the following equation:

$$\omega_s = \sqrt[3]{\frac{\omega_* (\rho_s - \rho) g v}{\rho}} \quad (8)$$

where ρ_s and ρ are densities (kg m^{-3}) of grain and fluid respectively, g is the gravitational acceleration (m s^{-2}), v is the kinematic viscosity of the fluid and ω_* is dimensionless particle settling velocity (-) which is estimated with an empirical equation:

$$\omega_* = R_3 \times 10^{R_1 + R_2} \quad (9)$$

where empirical coefficients R_1 , R_2 , and R_3 are calculated as

$$R_1 = -3.76715 + 1.92944 \log D_* - 0.09815 \log D_*^2 - 0.00575 \log D_*^3 + 0.00056 \log D_*^4 \quad (10)$$

$$R_2 = \left(\log \left(1 - \frac{1 - CSF}{0.85} \right) \right) \quad (11)$$

$$- (1 - CSF)^{2.3} \tanh(\log D_* - 4.6) + 0.3(0.5 - CSF)(1 - CSF)^{2.0}(\log D_* - 4.6) \quad (12)$$

$$R_3 = \left[0.65 - \left(\frac{CSF}{2.83} \tanh(\log D_* - 4.6) \right) \right]^{(1+(3.5-P)/2.5)} \quad (13)$$

where the values of Corey shape factor CSF (–) and the Powers roundness P (–) were set constants equal to 0.7 and 3.5 (typical coarse sand), and D_* is dimensionless nominal particle diameter calculated with the following formula:

$$D_* = \frac{(\rho_s - \rho)gD_n^3}{\rho v^2} \quad (14)$$

where D_n is the nominal diameter of a particle (m).

Suspended load flux was estimated for each ADCP transects as an average of suspended sediment concentration (SSC). For this estimate, we did not consider any and assumed that the water samples (near-surface, middle and near-bottom layers) capture the representative suspended load flux:

$$Q_R = \int_0^B SSC \cdot Q \cdot dB \quad (15)$$

Bedload fluxes (q_G) were estimated using a simplified formula for bedload transport, proposed by [28,29] and recalibrated on natural sand-bed river bedload transport data sets [30]

$$q_G = \varepsilon \rho_s V h \left(\frac{d_{50}}{h} \right)^{1.2} (M_e)^\eta \quad (16)$$

$$M_e = \frac{V - V_*}{\sqrt{R g d_{50}}} \quad (17)$$

The bedload in each cross-section was counted based on Q_G as

$$Q_G = \int_0^B q_G dB \quad (18)$$

Further partitioning between bed load and sediment load was assessed as $\frac{Q_R}{Q_R + Q_G}$ for each transect.

2.3. Grain Size and Hydrogeochemical Analyses

The water samples were then filtered for suspended material through a 0.45- μm membrane filter. The concentrations of elements were derived by inductively coupled plasma mass-spectrometry (ICP-MS) and atomic-emission spectroscopy (ICP-AES) methods. For the present study, we consider insoluble major elements (Fe, Al) and metals (Cd, Cr, Cu, Mo, Ni, Pb, As, Mn, Sr), which concentrations increase with decreasing grain size and hence are subject to hydrodynamic sorting. In addition, these elements are important regional pollutants [31].

Bottom sediments coarser than 1 mm were sieved manually to determine grain size. The finer sediment grain size was measured with a Fritsch Analysette 22 NanoTec Laser particle sizer (FRITSCH GmbH, Industriestrasse 8, 55743 Idar-Oberstein, Germany). All grain sizes were classified into 3 categories: clay (grain sizes $d < 5 \mu\text{m}$), silt ($d = 5\text{--}50 \mu\text{m}$), and sand ($>50 \mu\text{m}$). The average 50% (d_{50}) and 84% (d_{84}) sizes were also calculated for each sample. To calculate the d_{50} and d_{84} sediment particle diameters, the measured grain size distribution curves were linearized in double logarithmic coordinates, and the corresponding values were interpolated.

Particulate concentrations of metals c ($\mu\text{g/L}$) were determined based on the relative concentrations of elements within a sample C_0 ($\mu\text{g/g}$) accounting measured sediment concentrations SSC (g/m^3):

$$c = C_0 \cdot \text{SSC}/1000 \quad (19)$$

Further suspended load to bedload S-B analyses was used to characterize metals distribution over channel depth from the bottom (B) to suspended (S) sediments. Analyses of hydrodynamic sorting of a chemical within a vertical were done based on a ratio between concentrations of element x in the subsurface layer $C_{0\text{surf}}$ ($\mu\text{g/g}$) and near-bottom layer $C_{0\text{bot}}$ ($\mu\text{g/g}$):

$$Kx = C_{0\text{bot}}/C_{0\text{surf}} \quad (20)$$

Hence, $Kx > 1$ refers to hydrodynamic sorting of element x, whereas $Kx < 1$ is related to element x enrichment in the subsurface layers. We considered the sorting as homogenous when K_{SSC} varies as 1 ± 0.1 , and heterogeneous is $>1 \pm 0.3$. The Kx was also applied to physical parameters such as velocity V , d_{50} , SSC , and sand fractions share. This quantitative description of metals partitioning between the bed and suspended load is referred further as the suspended load to bedload analyses (SB-analyses). This approach develops DS-analyses related to partitioning between dissolved (D) and suspended (S) modes [31]. The exact quantitative descriptions of partitioning coefficients related to DS partitioning and SB partitioning are published initially in [32].

3. Results

3.1. Downstream Variations of Sediment Transport

Values of V^* corresponding to flow conditions during the time period of measurements presented herein (Figure 3b) demonstrate the shifted conditions of sediment transport. Both V^* , τ , and Ro demonstrate a decreasing trend along the river course, with an abrupt decline along the distributary river system (Figure 3).

The maximum streamflow discharge of the Selenga River that was measured by the ADCP unit at the delta apex on 28 July reached $2200 \text{ m}^3/\text{s}$. A comparison with the corresponding value at the gauging station showed only an 8% discrepancy between the gauge and the ADCP measurements. Figure 3 shows a significant alteration of hydraulic conditions between the main channel and the delta. All stream parameters rapidly decrease towards the delta edge. The smallest measured channels conveyed only 2%–4% of the main channel discharge.

The main channel (upstream of the delta), on the contrary, shows little streamflow variability—only 15% of the mean streamflow discharge ($1900 \text{ m}^3/\text{s}$). The mean water velocity also showed high stability—a 6% variance of the mean 1.8 m/s. The described contrast between the hydraulic conditions in the delta and the main Selenga River channel allows for a comparison of the sediment partitioning between the two reaches. Rouse number varies between maximum values within the transects S18–09 $Ro = 5.09$ in the upper part of the delta and $Ro = 0.01$ at one of the outer transects at the downstream part of the delta (transect S18–02). The values are ranged at certain parts of the river channel: they were between 0.01 and 1.04 at the vertical at delta edge transects, 0.06 and 5.21 (average $Ro = 1.55$) at delta channels transects, and from 0.11 to 3.84 (average $Ro = 2.81$) at the main channel upstream from the delta (transects from S18–17 to S18–28).

With changes in hydraulic conditions, the sediment transport mode is shifted along the three considered reaches. Assessment of the measured $Q_G + Q_R$ for each transect showed the downstream decrease of the sediment flux, therefore implying that some of the sediment must be depositing. In the main channel upstream from the delta, the $Q_R/(Q_G + Q_R)$ ratio variation lies between 10% and 30%, implying the dominant bedload transport conditions. In the most downstream part of the delta, the $Q_R/(Q_G + Q_R)$ ratio reaches 90%–100%. This increase of suspended sediment contribution to total transport along with the decline of the Rouse number value (see Figure 3b) is associated with the general increase of sediment sorting downstream. These variable conditions of sediment transport are clearly seen in the various grain-size sorting conditions observed in the delta (Figure 4) compared to upstream from the delta. In most profiles, particle distribution with depth displays a relatively

homogenous fashion. Particle coarsening with increasing depth is observed only at the delta edge where clay and silt particles are in the range of the critical sizes to be transported by the flow [8] and hence are settled. Clay particles are rather poorly sorted, especially along the upper part of the river, due to low settling velocities.

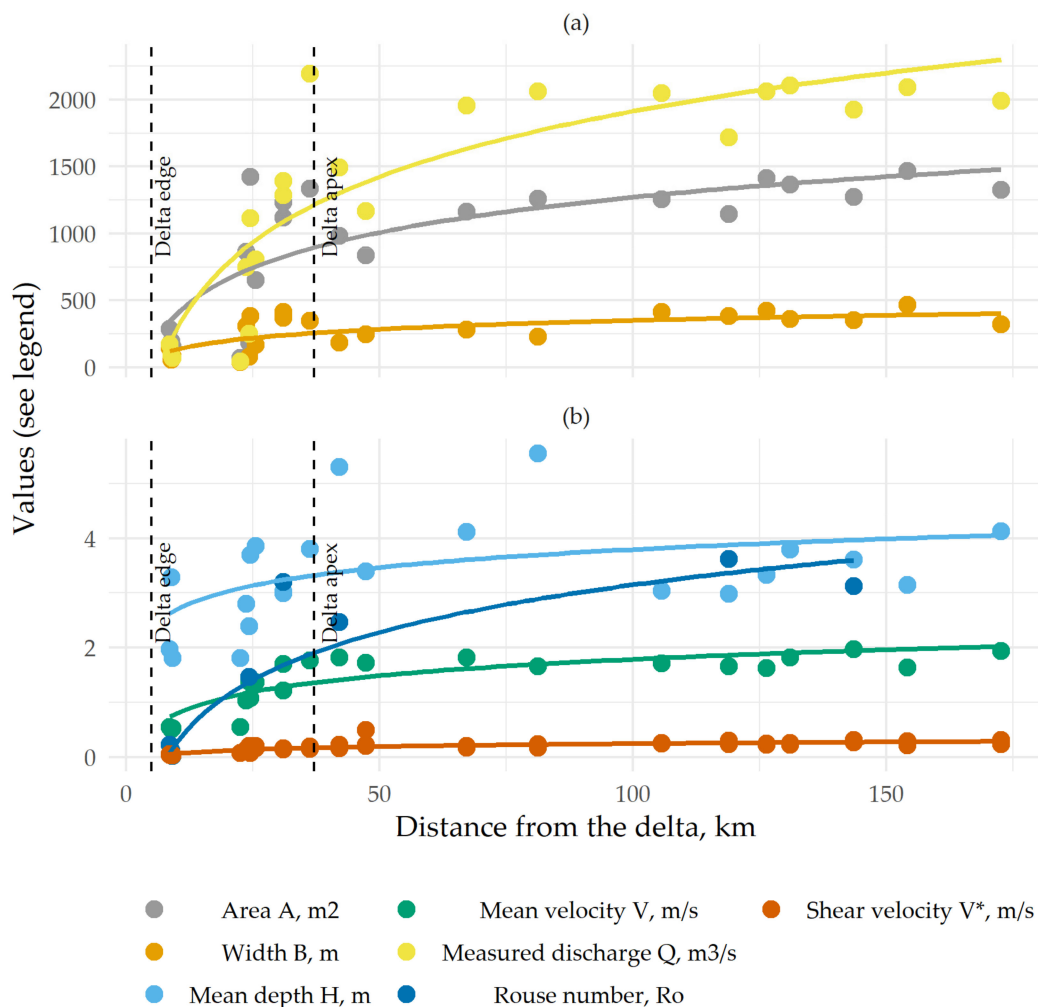


Figure 3. Hydraulic conditions along the examined river reach. Panels (a,b) show variables of different magnitude. Dashed lines show the delta edge and apex locations.

3.2. Sediment Grain Sizes and Geochemistry

The suspended sediments are poorly sorted in a range from 0.5 to 500 μm , with patterns specific to the delta channels (Figure 5a) and in the main channel (Figure 5b), with an average of 15 μm . Even though the average during the survey remained constant along a reach, some changes in the particular classes can be seen. The grain size mode is increasing from the surface to bottom sediments. In both patterns, grain sizes of suspended sediments are characterized by two dominant classes (bimodal pattern), both in near-surface, middle, and near-bottom samples (Figure 5). The first peak is associated with the 1–10- μm class, and the second belongs to 50–100 μm . Both in the delta and main channel, an increase of the coarser fractions (10–50 μm) is observed in the near-bottom sediments. Bed material samples generally have large mean diameters (several hundreds of μm) with a single-mode and evenly distributed along the spectrum from 1 to 100,000 μm . Finer bed material exists at the most downstream delta branches at the outlet, where due to sand and gravel termination upstream, only clay and silt particles are presented in the bottom layer (Figure 5b). Interestingly, the latter have the same grain size patterns as suspended sediments.

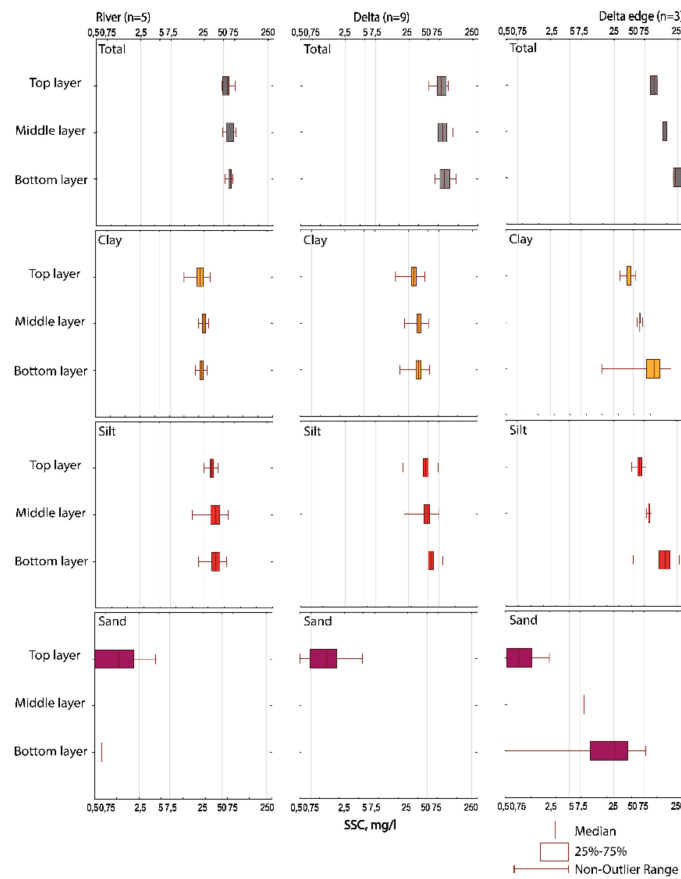


Figure 4. Composite vertical profiles of grain size distribution (total) and suspended sediment concentration fractions (clay, silt, and sand) of Selenga River (*n*—number of sampled verticals used to draft composite profile).

These grain size effects are clearly seen within the relative concentrations of elements C_0 ($\mu\text{g/g}$). The abundance of coarse particles, such as quartz or albite grains in the bottom sediments, decreases other element content. This dilution is maximal in the bottom where coarse-grained quartz concentration is maximum (Table 1). This implies that bottom sediments are enriched in elements such as Si, while suspended sediments are enriched in Al, Fe, and other elements carried in small or platy minerals such as micas or clays and associated with Al concentrations. Among studied elements, only Sr is not influenced by sediment sorting.

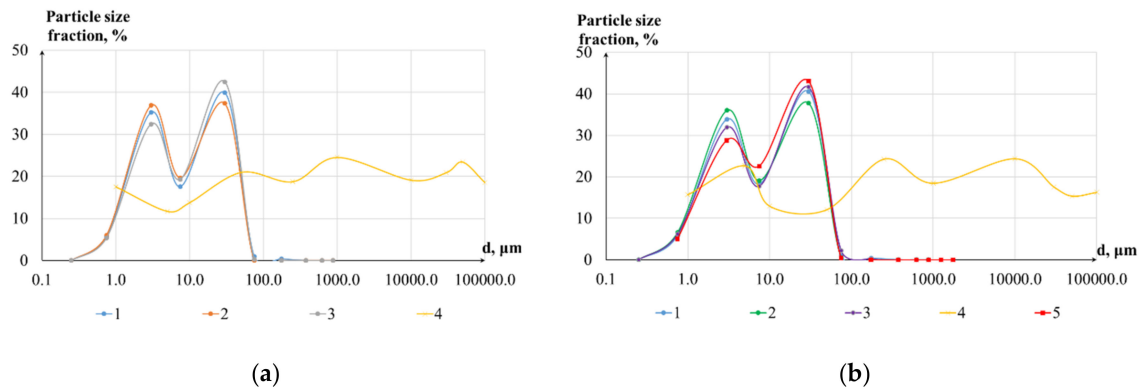


Figure 5. Composite vertical profile of grain size distribution in the delta channels (a) and in the main channel (b) of the suspended sediment (1—surface, 2—middle, 3—near-bottom layers) and bottom sediments (4). 5—average grain sizes of the bottom sediments at the delta edge transects.

Table 1. Composite relative concentrations of elements within sediment sample C_0 ($\mu\text{g/g}$).

Metal	Cd	Cu	Zn	Pb	Ni	Mo	As	Sr	Mn	Fe	Al
Suspended sediments	0.27	33	107	23.7	37.8	1.73	14.0	319	1345	46,811	79,107
Bottom sediments	0.08	6	44	12.5	7.7	0.47	2.5	338	334	13,422	61,969

The majority of the elements' concentrations mostly demonstrate an increasing trend along the studied reach. This might be due to higher discharge during sampling dates in the delta reach (Table 2). Under streamflow conditions of 2000–2200 m^3/s , the concentrations of most elements in the delta branches are 2–3 times higher compared to the adjacent upstream reach surveyed at 1800–2000 m^3/s . The most pronounced increase is related to near-bottom concentrations, which increased downstream, mostly with a factor of 3 (Table 2).

Table 2. Averaged concentrations of particulate metals c ($\mu\text{g/L}$) upstream from the river, in the delta, and in the delta edge.

Reach	Layer	V	Cd	Cr	Cu	Mo	Ni	Pb	As	Mn	Sr	Fe	Al
Main channel	top ($n = 5$)	mean	0.02	3.62	1.90	0.10	2.36	1.30	0.89	82.0	17.0	2669	4343
		\pm SD	0.00	0.44	0.15	0.01	0.23	0.14	0.15	6.00	3.00	221	455
	middle ($n = 5$)	mean	0.02	3.63	2.07	0.10	2.35	1.50	0.92	89.0	21.0	3005	5132
		\pm SD	0.00	0.43	0.27	0.02	0.30	0.22	0.08	10.0	4.0	343	798
	bottom ($n = 5$)	mean	0.02	3.38	2.07	0.10	2.45	1.43	0.81	86.0	18.0	2992	5036
		\pm SD	0.01	0.74	0.17	0.01	0.63	0.17	0.13	5.00	4.00	187	658
Delta	top ($n = 9$)	mean	0.02	4.67	2.74	0.14	3.02	1.96	1.16	109	25.0	3787	6278
		\pm SD	0.01	1.21	0.66	0.04	0.69	0.44	0.24	23.0	7.00	854	1658
	middle ($n = 8$)	mean	0.02	4.97	2.78	0.15	3.20	2.07	1.18	115	28.0	4018	6821
		\pm SD	0.00	1.14	0.58	0.04	0.66	0.41	0.23	23.0	8.00	803	1678
	bottom ($n = 8$)	mean	0.02	5.41	3.07	0.17	3.39	2.27	1.23	122	32.0	4298	7516
		\pm SD	0.01	1.13	0.60	0.04	0.71	0.40	0.23	24.0	8.00	853	1672
Delta edge	top ($n = 3$)	mean	0.03	6.70	3.58	0.21	4.02	2.60	1.56	145	35.0	5201	8795
		\pm SD	0.00	1.06	0.36	0.01	0.46	0.22	0.18	15.0	6.00	610	1357
	middle ($n = 3$)	mean	0.04	9.75	5.28	0.29	5.92	3.66	2.17	196	53.0	7207	12,704
		\pm SD	0.01	0.91	0.75	0.05	0.61	0.29	0.27	15.0	6.00	543	661
	bottom ($n = 3$)	mean	0.05	11.75	5.88	0.35	6.74	4.71	2.32	222	85.0	8763	18,172
		\pm SD	0.01	1.64	1.27	0.04	1.08	0.15	0.72	23.0	21.0	769	2601

A statistically significant increase in the concentration of metals in suspended sediments from the surface to the river bottom was revealed as an average for the whole considered river reach (Figure 6). The vertical distribution ratio (coefficient K_x , see Section 2.3) indicates that the physical characteristics of the flow are the most uniformly distributed over the depth parameters among all—flow velocity V , m/s ($K_v = 1.04$). Suspended sediment concentration SSC , mg/l , is characterized as heterogeneous and is lying within the range of metals concentrations value ($K_{\text{SSC}} = 1.12$). The metals can be ranked by the increase of the K_x value within the vertical profile in the following sequence: $\text{Pb-As-Mn-Mo-Cr-Ni-Cu-Cd}$. The value of K_x varies from $K_{\text{Pb}} = 1.04$ to $K_{\text{Cd}} = 1.42$. These effects are different for the particular river reaches. Rather homogenous metals distribution or even decrease of concentrations ($K_x < 1$) over depth are observed in the upper channel reach upstream from the delta consistently with an observed increase of the bedload transport and coarsening of the near-bottom suspended sediments. In the delta where no sand or gravel transport is observed, the concentrations of metals increase in the near-bottom layer, both with increases of metal-bearing clay and silt fractions.

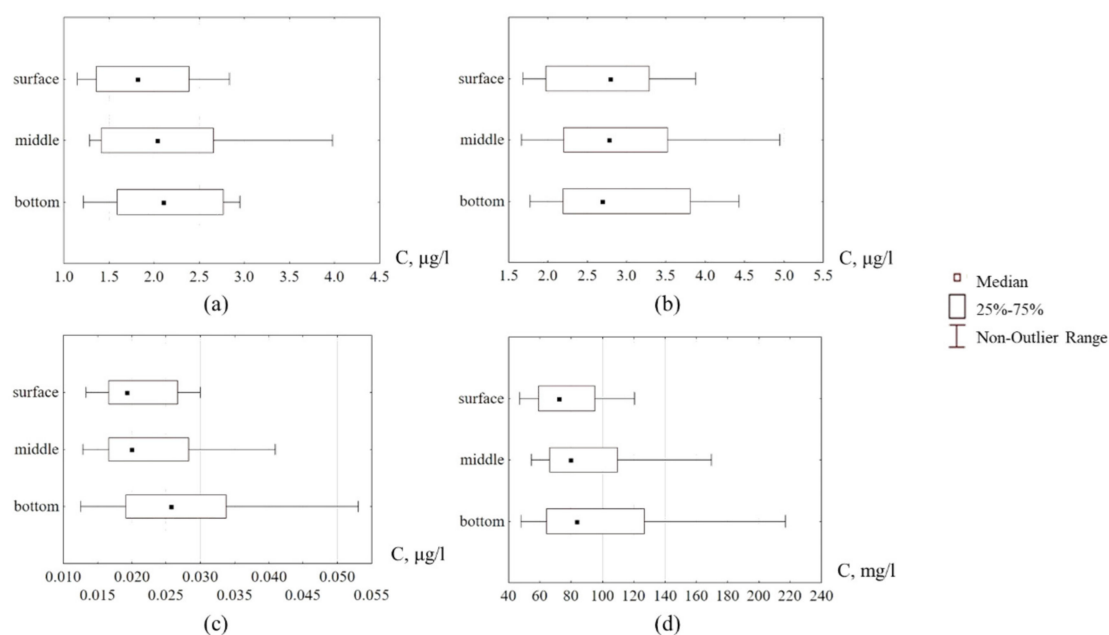


Figure 6. Composite particulate concentration c ($\mu\text{g/l}$) of Pb (a), Cu (b), Cd (c), and SSC (d) in suspended sediments versus depth in the Selenga River from Ulan-Ude to delta edge in 2018.

The role of hydrodynamic sorting of grain sizes due to changing runoff conditions is clearly seen by the relationship between particulate concentrations and grain sizes (Table 3). The distribution of the metals within the depth column is mostly due to hydrodynamic sorting of grain sizes. Most chemical elements (both major elements—Na, Mg, K, Ca, Al, Fe, and Mn—and metals) show strong relations between grain-size and chemical composition [33–36]. Under the conditions of the hydrodynamic sorting, we observed significant correlations ($R_{\text{cor}} > 0.5$, p -values < 0.001) between size fraction 0.5–1 μm for most of the elements (Table 3). Most elements show strong relations between grain-size and chemical composition (Figure 7). This can be explained both by typical enrichment of clay fractions by the metals (as have been shown by various regional studies demonstrating the crucial role of $<16\text{-}\mu\text{m}$ sediments in transporting metals [37]. Also elevated correlations ($\bar{R}_{\text{cor}} > 0.60$, $p < 0.001$, $n = 33$) were observed with the 50–100- μm size fraction. The latter emphasize the possible role of coarser sediments (silt–sand) due to other speciation of metals related to minerals. Examples of bimodal distribution with sediment grain sizes can be found in literature in relation to Fe-Mn oxides, which can drive variation of relative distribution percentage for each metal speciation (Cu, Ni, Pb, Cr, and Zn) at a primary binding phase in sediment particles [36].

Table 3. Correlation matrix (%) of relations between grain classes and particulate concentrations of metals.

Particle Size Fraction, μm	Al	As	Cd	Cr	Cu	Fe	Mn	Mo	Ni	Pb	Sr	SSC, mg/l
<0.5	−13	−7	−12	−9	−12	−14	−12	−13	−9	−13	−10	−9
0.5–1	61	48	40	51	48	61	49	50	51	53	53	57
1–5	−30	−23	−40	−31	−28	−23	−31	−32	−28	−33	−38	−32
5–10	−51	−37	−42	−46	−41	−44	−43	−46	−43	−49	−55	−54
10–50	2	13	23	13	15	2	15	14	11	12	10	−1
50–100	62	33	46	47	40	48	44	47	44	53	67	70
100–250	5	−9	−2	−2	−7	−4	−5	−2	−3	1	11	17
250–500	−19	−17	−14	−16	−18	−21	−18	−18	−16	−18	−16	−15

Bold dashed values are with $R_{\text{cor}} \geq 0.5$.

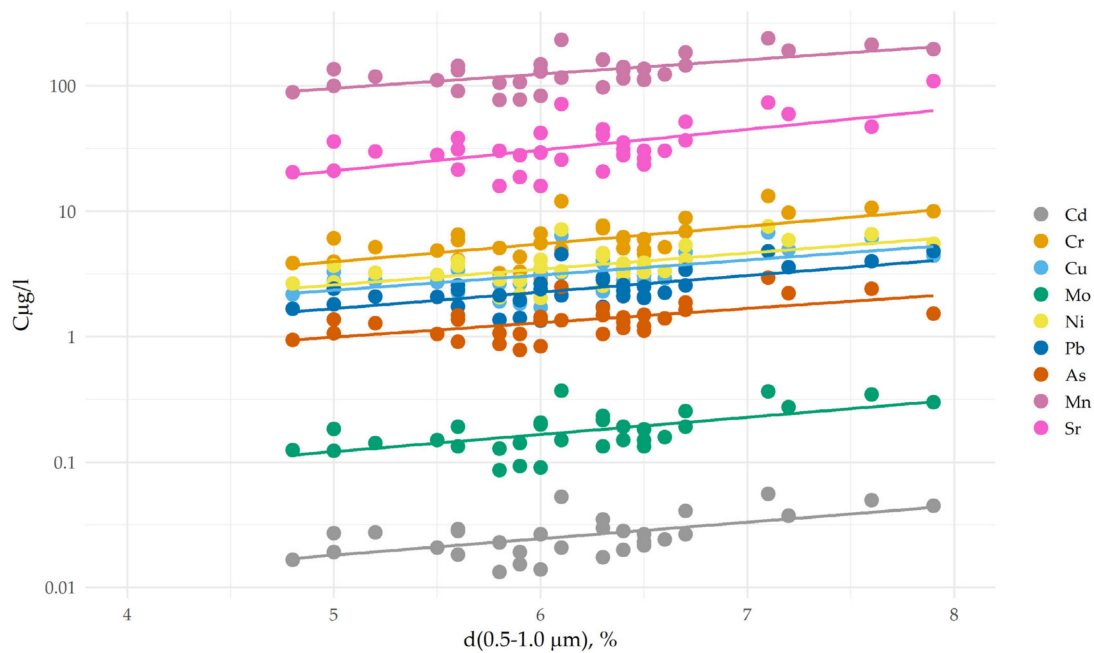


Figure 7. Relation between element particulate concentrations of metals c ($\mu\text{g/L}$) and grain size 0.5–1 μm content (% from total weight of the sample, $\bar{r}_{\text{cor}} > 0.60$, $p < 0.001$, $n = 33$).

4. Discussion

4.1. Bed and Suspended Sediment Fluxes

The calculations indicate that sediment flux decreases downstream with an increasing bifurcation in the delta [8], which generally corresponds with the previous studies and also the hypothesis of gravel termination [20]. The latter can be responsible for the abrupt decline in bedload flux, which almost stops in the delta outlets. Shear stress and Rouse number are also reduced downstream due to water partitioning among the bifurcating channels. As one can see from the obtained datasets, the shear stress, which is not sufficient to produce gravel transport for the delta channels, also induces depositional patterns in the suspended sediment flux: the increase of near-bottom concentrations is the evidence of downward fluxes of the most suspended particles, also including most fine clay particles.

The hydrodynamic gradient lays within the threshold for bedload transport conditions. Generally, it is assumed that for the rivers with a similar size as Selenga, values lower than the critical Rouse number $Ro^* = 2.5$ indicate that a sediment particle begins to contribute to the suspended load [38,39], whereas higher values indicate that a sediment particle is most likely transported as part of the bedload [40]. To test the relationship between the observed Ro numbers, we plotted our results (Figure 8) of the relationship between the ratio of suspended load to total load and Rouse number based on the laboratory data for the mixed load from Guy, Simons, and Richardson [41]. Lines shown are those from the Einstein integrals of Guo and Julien, as obtained by Shah-Fairbank [42] for h/d 100 and 100.000. It can be clearly seen that the measured conditions in the Selenga River are generally close to fit line for the rivers at $h/d_{50} = 100.000$. At the same time, this shows that one can obtain an extremely large variability in sediment concentration and thus the $Q_R/(Q_G + Q_R)$ ratio in deep sand-bed rivers when the Rouse number is fairly large ($Ro > 0.5$). The case study on Selenga River is quite instructive in this regard, which reflects conditions of the abrupt shift from a mixed load and bedload dominated channel ($Ro < 2$) to a suspended sediment dominated channel ($Ro > 2$).

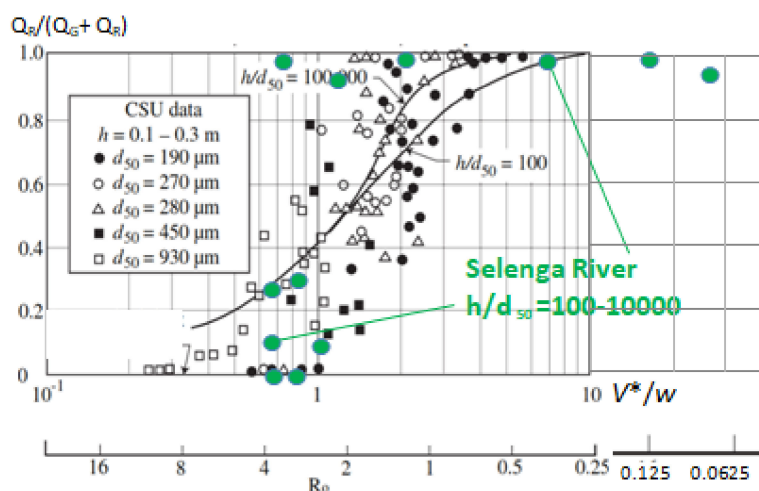


Figure 8. The observed values of Ro and partitioning conditions of sediment transport $Q_R/(Q_G + Q_R)$ within the Selenga River compared to experimental data [43].

4.2. Particulate Metals Behavior and SB-Analyses

Both hydrodynamic (stream velocities) and hydrological (water discharge rates) impacts can explain the patterns of particulate metals along the Lower Selenga River. Absolute concentrations along the river course are mostly driven by temporal changes of water discharge during flood propagation. The latter significantly influences the increase of particulate concentrations in the delta compared to the upper adjacent main channel reach. This fact, which contradicts previous observations on suspended sediment retention within a delta [8,19] and storage of particulate and dissolved chemicals [18], can be explained by the extensive role of storm events in geochemical flows. As it was shown in the previous regional studies [44], relatively fine particles (62–250 μm ; particle size 1) are eroded preferentially over coarser particles during the high flow events, implying their prevalence in suspension during these high flow conditions. Vice versa, these fine fractions are most important in the transport of metals [6,45], and, thus, overall trends of concentrations increase are consistent among the different heavy metals, although the magnitude of change differs. This implies an important consideration that the delta function as a geochemical buffer is time- and discharge-dependent. This statement is in general agreement with the contrasting sedimentation patterns observed via satellite images [19], which reveal sediment storage (a downward decline of sediment transport) in the Selenga delta during high discharges ($>1500 \text{ m}^3/\text{s}$). Sediment concentrations increase can be seen under lower streamflow conditions ($<1500 \text{ m}^3/\text{s}$). This might be particularly important due to observed influence of climate change on the seasonal discharges of the Selenga River [46–48], which cause a significant impact on channel processes in the lower reaches of the river [32] and chemical composition due to the drought period observed for the last 20 years [49,50].

We performed a quantitative description of metals partitioning between the bed and suspended fluxes (SB-analyses) using the ratio between concentrations of element x in the subsurface layer and near-bottom layer K_x (see Section 2.3). This parameter significantly varied along the transition zone from the sand-gravel of the Selenga River to the sandy-silt channels of the delta area, where the depositional pattern led to higher sorting of fine metal-bearing fractions. For element concentrations, K_x increased significantly in the delta channels (Table 4). The hydrodynamic structure of the flow remains largely unchanged (a decrease in velocities from the surface to the bottom is characterized by a similar ratio $K_v = 0.94$ upstream of the delta and $K_v = 0.96$ in the delta), while the average velocity decreases steadily downstream the delta area (see Figure 3). The leading factor in the formation of the heavy metal transfer pattern as a suspended load should be considered in the peculiarities of the mass transfer between the channel flow and bottom sediments, which differs depending on the type of sediment that the channel consists of. On average, in the delta sandy-silt channels, the increase

in heavy metals concentration in suspended sediment is 30%–40% higher than in the Selenga River main channel. These gradients can be associated with a larger concentration of fine silt at the bottom of the floodplain channels, and the deposition of heavier sand mineral fractions containing metals in their crystal lattice. At the same time, the SSC gradient in the delta channels increases even more significantly ($K_{SSC} = 1.75$ in the delta versus $K_{SSC} = 0.99$ in the main channel). The tremendous role of larger mineral fractions sedimentation in the formation of vertical heterogeneity is confirmed by the sand fraction ($>50 \mu\text{m}$) content increase in the composition of the bottom sediments of the delta channels ($K_{\text{Sand}} (\%) = 1.75$).

Table 4. Ratio between chemical (I) and physical (II) parameters of particulate matter and flow in the surface layer and near-bottom layer (K_x according to Equation (18) along the Selenga River).

Location	I											II			
	C											V	d50	Sand	SSC
	Cd	Cr	Cu	Mo	Ni	Pb	As	Mn	Se	Fe	Al				
Delta channels	1.40	1.31	1.31	1.38	1.33	1.40	1.22	1.28	1.72	1.35	1.54	0.96	1.05	1.75	1.75
Main channel	0.93	1.09	1.09	1.07	1.04	1.10	0.91	1.04	1.08	0.84	0.87	0.94	0.9	0.43	0.99
Whole research area	1.29	1.26	1.26	1.31	1.26	1.33	1.14	1.22	1.58	1.25	1.41	0.95	0.99	1.11	1.57

Calculations of K_x were done. I: C—concentrations of elements. II: V—stream velocity; d50—50% grain size; Sand—content of sand; SSC—suspended sediment concentration.

Finally, we accounted for impacts of hydrodynamic conditions and sediment partitioning on metals distribution within the depth column using joint analyses of R_o and K_x numbers (Figure 9). Due to the high variability of R_o under transient conditions of the channel–delta interface and also unsteady flow during flood propagation, we were not able to obtain significant relationships between hydrodynamic parameters and geochemical coefficients. Nevertheless, Figure 9 clearly demonstrates the increase of the metals in the near-bottom layers at the low values of R_o (dominant suspended mode of transport) and fits the following relationship ($R_{\text{cor}} = -0.32$, $p\text{-value} < 0.001$, $n = 150$):

$$K_x = 1.25 R_o^{-0.077}. \quad (21)$$

The observed pattern can be explained by the absence of coarser fractions in the near-bottom layer due to sand and gravel termination in the upper part of delta [7]. Vice versa, a strong sorting of clay particles under low R_o values conditions became the crucial driver of K_x increase. Hence we can conclude that grain size sorting varied between suspended load and bedload dominated river reaches. In the suspended dominated reach, a clearer sorting of fine particles is observed, which explains the metals' behavior and sorting along the depth profile. In some samples, small portions of sand were also observed in the delta edge, which is mostly explained by its possible delivery from the eroded bank during the flood propagation. Upstream from the delta in the main channel of the Selenga River, the hydrodynamic enrichment of relatively coarse quartz grains near the bottom of the channel can be attributed to observed low values of K_x . Unfortunately, at this point, we did not collect enough samples to prove this statement with a sufficient number of grain size profiles.

The observed patterns of hydrodynamic grain size and metal sorting do not have unique patterns and depend on the hydrodynamic conditions of sediment transport. In similar hydrodynamic conditions with low Rouse number and dominant suspended load, as observed in the case of the Selenga delta, K_x typically has values >1 . In the Ganges River, the trace elements in the suspended load As, Ba, Bi, Co, Cr, Cs, Cu, Ga, Rb, V and Zn concentrations were negatively correlated with d84 grain size and were higher in the suspended load compared to bedload samples [6], indicating high numbers of K_x within a vertical profile. Vice versa, in the case of bedload-dominated rivers—the

Amazon River and its tributaries [5] and Yangtze River [51]—the K_x value is significantly lower than 1. Here the amount of quartz in the samples is the main factor controlling the concentration of these elements throughout the sampled depth profiles due to hence so-called “quartz dilution effect” [5]. This interrelation between mineralogy and grain size is due to the fact that quartz as a mineral is mostly related to coarser sand sediments ($>50 \mu\text{m}$ or larger), which is proved by empirical evidence worldwide (e.g., [33]). The absence of a significant correlation between K_x and R_o for any of the elements x can be attributed to unsteady flow conditions during flood propagation. Another example was found at the Yellow River flow [51] under conditions of the sand-dominated suspended load. Here due to the possible impact of artificial flood from the reservoir, the extremely high-velocity profiles lead to suspension and diffusion of coarse sand material, which also leads to relatively low values ($K_x < 1$).

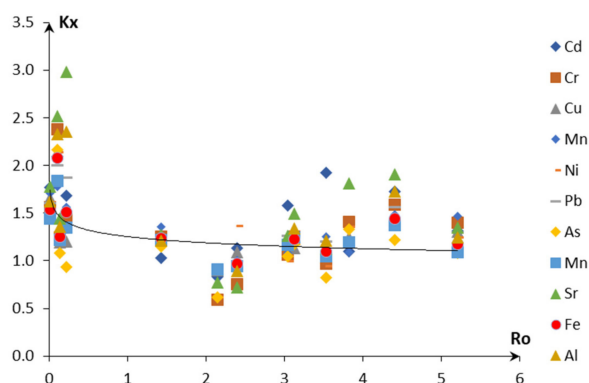


Figure 9. Relationship between coefficient of vertical metal concentrations heterogeneity K_x and Rouse number R_o ($R_{cor} = -0.32$, p -value < 0.001 , $n = 150$).

The revealed patterns are important for organizing surface water monitoring and assessing the transformation of pollutant fluxes along the river. Existing studies, which rely on single surface water samplings, are associated with large uncertainties. These approaches can be characterized by the incompatibility of datasets obtained for various river reaches. For instance, at the reaches where $K_x \ll 1$ or $K_x \gg 1$, surface water sampling will induce high errors in particulate fluxes' estimates. For the Baikal region in particular, the hydroclimatic impact on metals spreading may significantly influence pollutant delivery into the Lake Baikal. Regional climate change has been proven to influence the magnitude and number of extreme flow events [47]. Thus, the impact on sediment storage during these events may be significantly changed compared to previous conditions due to enhanced depositional or erosional processes.

Finally, we conclude that consideration of hydrodynamic conditions is of primary importance for sediment quality monitoring design.

5. Conclusions

We revealed the sorting impact on erosion products and associated heavy metals by river flow due to interaction between the transient flow and channel bed (near-bottom sediments (bedload) and bottom deposits). The following main conclusions are drawn:

1. Due to hydrodynamic impacts of varying channel patterns along the river continuum, various patterns of heavy metals are observed along the river course. Depositional channels such as Selenga delta branches act as a better “sorting machine” of heavy metals (30% to 40% vertical distribution is higher in the delta than in the gravel-boulder main channel of the Selenga river).
2. This increase can be attributed to a higher concentration of the clay-silt fraction near the bed in the deltaic channels due to its heavier mineral structure containing specific microelements. The SSC gradient towards the bottom is further pronounced ($K_{ssc} = 1.75$ vs. $K_{ssc} = 0.99$ in the main channel).

- This vertical variability is also caused by the pronounced increase of coarse mineral fractions (50–2000 mm) in the near-bottom layer in the depositional delta pattern ($K(\text{sand } (\%)) = 1.75$) compared to the unbraided main stem of the Selenga river where sediments are deposited on the bottom, thus having increased content in the near-bottom layers.

Author Contributions: The work was conceived by S.C. The text was mostly written by S.C., V.M. and E.S. V.M. and E.S. were responsible for field data collection and processing. V.E. and L.E. did the hydrochemical data processing. S.C., M.L. and N.K. provided general supervision of the project and editing. All authors have read and agreed to the published version of the manuscript.

Funding: Field studies were supported by the Russian Fund for Basic Research (project17-29-05027) and the RFBR-Russian Geographical Society project (RFBR-17-05-41174-RGS); sampling methodology was developed as a part of RFBR project 18-05-60219. Channel processes analyses were done under the Russian Scientific Foundation project 18-17-00086.

Acknowledgments: The authors thank all members of the Faculty of Geography of LMSU who participated in the field studies or performed analytical work. Research was done with technical support of the Joint Russian-Mongolian complex biological expedition and the Baikal Institute of Nature Management Siberian Branch of the Russian Academy of Sciences (BINM SB RAS).

Conflicts of Interest: The authors declare no conflicts of interest. The funders had no role in the design of the study; in the collection, analyses, or interpretation of data; in the writing of the manuscript, or in the decision to publish the results.

References

- Horowitz, A.J.; Rinella, F.A.; Lamothe, P.; Miller, T.L.; Edwards, T.K.; Roche, R.; Rickert, D.A. Variations in Suspended Sediment and Associated Trace Element Concentrations in Selected Riverine Cross Sections. *Environ. Sci. Technol.* **1990**, *24*, 1313–1320. [[CrossRef](#)]
- Rouse, H. *Fluid Mechanics for Hydraulic Engineers*, 1st ed.; McGraw-Hill: New York, NY, USA, 1938.
- Dupré, B.; Gaillardet, J.; Rousseau, D.; Allègre, C.J. Major and trace elements of river-borne material: The Congo Basin. *Geochim. Cosmochim. Acta.* **1996**, *60*, 1301–1321. [[CrossRef](#)]
- Meybeck, M.; Ragu, A. *River Discharges to the Oceans: An Assessment of Suspended Solids, Major Ions and Nutrients*; UNEP: Nairobi, Kenya, 1997; pp. 3–14.
- Bouchez, J.; Maurice, L.; France-Lanord, C.; Dutra-Maia, P.; Gaillardet, J. Grain size control of river suspended sediment geochemistry: Clues from Amazon River depth profiles. *Geochem. Geophys. Geosystems.* **2011**, *12*, 12. [[CrossRef](#)]
- Lupker, M.; France-Lanord, C.; Lavé, J.; Bouchez, J.; Galy, V.; Métivier, F.; Gaillardet, J.; Lartiges, B.; Mugnier, J.-L. A Rouse-based method to integrate the chemical composition of river sediments: Application to the Ganga basin. *J. Geophys. Res. Space Phys.* **2011**, *116*, 116. [[CrossRef](#)]
- Dong, T.Y.; Nittrouer, J.A.; Il'icheva, E.; Pavlov, M.; McElroy, B.; Czapiiga, M.J.; Ma, H.; Parker, G. Controls on gravel termination in seven distributary channels of the Selenga River Delta, Baikal Rift basin, Russia. *GSA Bull.* **2016**, *128*, 1297–1312. [[CrossRef](#)]
- Pietroń, J.; Nittrouer, J.A.; Chalov, S.R.; Dong, T.Y.; Kasimov, N.; Shinkareva, G.; Jarsjö, J. Sedimentation patterns in the Selenga River delta under changing hydroclimatic conditions. *Hydrol. Process.* **2018**, *32*, 278–292. [[CrossRef](#)]
- Karthe, D.; Chalov, S.; Gradel, A.; Kusbach, A. Special issue «environmental change on the Mongolian plateau: Atmosphere, forests, soils and water». *Geogr. Environ. Sustain.* **2019**, *12*, 60–65. [[CrossRef](#)]
- Shinkareva, G.L.; Lychagin, M.Y.; Tarasov, M.K.; Pietroń, J.; Chichaeva, M.A.; Chalov, S.R. Biogeochemical specialization of macrophytes and their role as a biofilter in the Selenga delta. *Geogr. Environ. Sustain.* **2019**, *12*, 240–263. [[CrossRef](#)]
- Garmaev, E.Z.; Kulikov, A.I.; Tsydyrov, B.Z.; Sodnomov, B.V.; Ayurzhanayev, A.A. Environmental Conditions of Zakamensk Town (Dzhida River Basin Hotspot). *Geogr. Environ. Sustain.* **2019**, *12*, 224–239. [[CrossRef](#)]
- Timofeev, I.V.; Kosheleva, N.E.; Kasimov, N.S.; Gunin, P.D.; Sandag, E.-A. Geochemical transformation of soil cover in copper–molybdenum mining areas (Erdenet, Mongolia). *J. Soils Sediments.* **2015**, *16*, 1225–1237. [[CrossRef](#)]
- Chalov, S.R.; Thorslund, J.; Kasimov, N.; Aybullatov, D.; Ilyicheva, E.; Karthe, D.; Kositsky, A.; Lychagin, M.; Nittrouer, J.; Pavlov, M.; et al. The Selenga River delta: a geochemical barrier protecting Lake Baikal waters. *Reg. Environ. Chang.* **2016**, *17*, 2039–2053. [[CrossRef](#)]

14. Popovskaya, G.I.; Tashlykova, N.A. *The Selenga River Delta—Natural Biofilter and Indicator of the Condition of Lake Baikal*; Tulokhonov, A.K., Ed.; Publishing house of SB RAS: Novosibirsk, Russia, 2008; pp. 167–181.
15. Chalov, S.R.; Potemkina, T.G.; Pashkina, M.P.; Kasimov, N.S. Evolution of Suspended Sediment Budget in the Deltas of Lake Baikal Tributaries. *Russ. Meteorol. Hydrol.* **2019**, *44*, 667–673. [[CrossRef](#)]
16. Ivanov, V.V.; Korotayev, V.N.; Labutina, I.A. *Morphology and Dynamics of the Selenga River Delta*; Vestnik Moskovskogo Universiteta: Moscow, Russia, 2007; pp. 48–54.
17. Sinyukovich, V.N. The water balance of the Selenga river basin. *Geogr. Nat. Resour.* **2008**, *29*, 54–56. [[CrossRef](#)]
18. Chalov, S.; Golosov, V.; Tsyplenkov, A.; Theuring, P.; Zakerinejad, R.; Märker, M.; Samokhin, M. A toolbox for sediment budget research in small catchments. *Geogr. Environ. Sustain.* **2017**, *10*, 43–68.
19. Chalov, S.R.; Bazilova, V.O.; Tarasov, M.K. Modelling suspended sediment distribution in the Selenga River Delta using LandSat data. *Proc. Int. Assoc. Hydrol. Sci.* **2017**, *375*, 19–22. [[CrossRef](#)]
20. Dong, T.; Nittrouer, J.A.; Czapiga, M.J.; Ma, H.; McElroy, B.; Il'Icheva, E.; Pavlov, M.; Chalov, S.; Parker, G. Roles of Bank Material in Setting Bankfull Hydraulic Geometry as Informed by the Selenga River Delta, Russia. *Water Resour. Res.* **2019**, *55*, 827–846. [[CrossRef](#)]
21. Gyninova, A.B.; Korsunov, V.M.; Beshentsev, A.N.; Balsanova, L.D.; Ubugunova, V.I.; Gyninova, B.D. Accumulation of substances on geochemical barriers in the Selenga delta. *Geogr. Nat. Resour.* **2007**, *2*, 65–69.
22. Sorokovikova, L.M.; Popovskaya, G.I.; Sinyukovich, V.N.; Tomberg, I.V.; Bashenkhaeva, N.V.; Tashlykova, N.A. Water chemistry and phytoplankton in water bodies in the Selenga River's delta under ice cover. *Water Resour.* **2006**, *33*, 321–328. [[CrossRef](#)]
23. Karthe, D.; Kasimov, N.S.; Chalov, S.R.; Shinkareva, G.L.; Malsy, M.; Menzel, L.; Theuring, P.; Hartwig, M.; Schweitzer, C.; Hofmann, J.; et al. Integrating multi-scale data for the assessment of water availability and quality in the Kharaa - Orkhon - Selenga river system. *Geogr. Environ. Sustain.* **2014**, *7*, 65–86. [[CrossRef](#)]
24. Parker, G. The uses of sediment transport and morphodynamic modeling in stream restoration. In Proceedings of the 2004 World Water and Environmental Resources Congress: Critical Transitions in Water and Environmental Resources Management, Salt Lake City, UT, USA, 27 June–1 July 2004; pp. 812–815.
25. Whiting, P.J.; Dietrich, W.E. Convective accelerations and boundary shear stress over a Channel Bar. *Water Resour. Res.* **1991**, *27*, 783–796. [[CrossRef](#)]
26. Wilcock, P.R. Estimating local bed shear stress from velocity observations. *Water Resour. Res.* **1996**, *32*, 3361–3366. [[CrossRef](#)]
27. Dietrich, E.W. Settling Velocity of Natural Particles. *Water Resour. Res.* **1982**, *18*, 1615–1626. [[CrossRef](#)]
28. Van Rijn L., C. *Principles of Sediment. Transport. in Rivers, Estuaries and Coastal Seas*; Aquapublications: Blokzijl, The Netherlands, 1993; pp. 1–17.
29. Van Rijn, L.C. Sediment Transport, Part I: Bed Load Transport. *J. Hydraul. Eng.* **1984**, *110*, 1431–1456. [[CrossRef](#)]
30. Van Rijn, L.C. Unified View of Sediment Transport by Currents and Waves. I: Initiation of Motion, Bed Roughness, and Bed-Load Transport. *J. Hydraul. Eng.* **2007**, *133*, 649–667. [[CrossRef](#)]
31. Kasimov, N.; Kosheleva, N.; Lychagin, M.; Chalov, S.R.; Alekseenko, A.V.; Bazilova, V.; Beshentsev, A.; Bogdanova, M.; Chernov, A.V.; Dorjgotov, D.; et al. *Environmental Atlas Selenga-Baikal*; Faculty of Geography, Lomonosov Moscow State University: Moscow, Russia, 2019; p. 288.
32. Chalov, S.R.; Jarsjö, J.; Kasimov, N.; Romanchenko, A.; Pietron, J.; Thorslund, J.; Belozeroval, E. Spatio-temporal variation of sediment transport in the Selenga River Basin, Mongolia and Russia. *Environ. Earth Sci.* **2014**, *73*, 663–680. [[CrossRef](#)]
33. Horowitz, A.J. *Primer on Trace Metal-Sediment Chemistry*; US Government Printing Office: Washington, DC, USA, 1985; p. 2277.
34. Horowitz, A.; Elrick, K.A. The relation of stream sediment surface area, grain size and composition to trace element chemistry. *Appl. Geochem.* **1987**, *2*, 437–451. [[CrossRef](#)]
35. Miller, J.; Lechler, P.J.; Mackin, G.; Germanoski, D.; Villarroel, L.F. Evaluation of particle dispersal from mining and milling operations using lead isotopic fingerprinting techniques, Rio Pilcomayo Basin, Bolivia. *Sci. Total. Environ.* **2007**, *384*, 355–373. [[CrossRef](#)]
36. Tansel, B.; Rafiuddin, S.; Tansel, B.; Rafiuddin, S. Heavy metal content in relation to particle size and organic content of surficial sediments in Miami River and transport potential. *Int. J. Sediment. Res.* **2016**, *31*, 324–329. [[CrossRef](#)]

37. Yao, Q.; Wang, X.; Jian, H.; Chen, H.; Yu, Z. Characterization of the particle size fraction associated with heavy metals in suspended sediments of the yellow river. *Int. J. Environ. Res. Public Health*. **2015**, *12*, 6725–6744. [[CrossRef](#)]
38. Middleton, G.V.; Southard, J.B. *Mechanics of Sediment. Movement*; SEPM Society for Sedimentary Geology: Tulsa, OK, USA, 1984.
39. Huston, D. Particulate organic carbon trapping efficiency in the stream bed for cobbles and gravels: A laboratory test. *Kaleidoscope* **2014**, *11*, 73.
40. Lynds, R.M.; Mohrig, D.; Hajek, E.A.; Heller, P.L. Paleoslope Reconstruction in Sandy Suspended-Load-Dominant Rivers. *J. Sediment. Res.* **2014**, *84*, 825–836. [[CrossRef](#)]
41. Guy, H.; Simons, D.; Richardson, E. *Summary of Alluvial Channel Data from Flume Experiments 1956–1961*; US Government Printing Office: Washington, DC, USA, 1966; pp. 1–104.
42. Shah-Fairbank, S.C.; Julien, P.Y. Sediment load calculations from point measurements in sand-bed rivers. *Int. J. Sediment. Res.* **2015**, *30*, 1–12. [[CrossRef](#)]
43. Julien, P.Y. *Erosion and Sedimentation*, 2nd ed.; Cambridge University Press: Cambridge, UK, 2010; p. 371.
44. Pietroń, J.; Jarsjö, J.; Romanchenko, A.O.; Chalov, S.R. Model analyses of the contribution of in-channel processes to sediment concentration hysteresis loops. *J. Hydrol.* **2015**, *527*, 576–589. [[CrossRef](#)]
45. Bouchez, J.; Métivier, F.; Lupker, M.; Maurice, L.; Pérez, M.; Gaillardet, J.; France-Lanord, C. Prediction of depth-integrated fluxes of suspended sediment in the Amazon River: Particle aggregation as a complicating factor. *Hydrol. Process.* **2010**, *25*, 778–794. [[CrossRef](#)]
46. Antokhina, O.Y.; Latysheva, I.V.; Mordvinov, V.I. A Cases Study of Mongolian Cyclogenesis during the July 2018 Blocking Events. *Geogr. Environ. Sustain.* **2019**, *12*, 66–78. [[CrossRef](#)]
47. Frolova, N.; Belyakova, P.; Grigor'Ev, V.Y.; Sazonov, A.A.; Zotov, L.V. Many-year variations of river runoff in the Selenga basin. *Water Resour.* **2017**, *44*, 359–371. [[CrossRef](#)]
48. Moreido, V.M.; Kalugin, A.S. Assessing possible changes in Selenga R. water regime in the XXI century based on a runoff formation model. *Water Resour.* **2017**, *44*, 390–398. [[CrossRef](#)]
49. Sorokovikova, L.M.; Sinyukovich, V.N.; Tomberg, I.V.; Popovskaya, G.I.; Chernyshev, M.S.; Ivanov, V.G.; Khodzher, T.V. The status of the aquatic ecosystem of the Selenga river delta under long-duration low-water conditions. *Geogr. Nat. Resour.* **2017**, *38*, 60–67. [[CrossRef](#)]
50. Tomberg, I.V.; Sorokovikova, L.M.; Sinyukovich, V.N.; Pogodaeva, T.V. Ion flow in the Selenga river Delta under low water content conditions. *Meteorol. Hydrol.* **2006**, *12*, 87–95.
51. Qiao, S.; Yang, Z.; Pan, Y.; Guo, Z. Metals in suspended sediments from the Changjiang (Yangtze River) and Huanghe (Yellow River) to the sea, and their comparison. *Estuarine Coast. Shelf. Sci.* **2007**, *74*, 539–548. [[CrossRef](#)]

